Light Metals 2013 *Edited by: Barry Sadler*
TMS (The Minerals, Metals & Materials Society), 2013

GRAIN SUBDIVISION AND ITS EFFECT ON TEXTURE EVOLUTION IN AN ALUMINUM ALLOY UNDER PLANE STRAIN COMPRESSION

Q. Ma[1], W. Mao[2], B. Li[1], P.T. Wang[1], M.F. Horstemeyer[1,3]

[1]. Center for Advanced Vehicular Systems, Mississippi State University, Starkville, MS 39759, USA
[2]. Department of Materials Science, University of Science and Technology Beijing, Beijing, 100083, China
[3]. Department of Mechanical Engineering, Mississippi State University, Starkville, MS 39762, USA

Keywords: Aluminum; Texture; Deformation; Grain subdivision; EBSD.

Abstract

Grain subdivision is widely observed in plastic deformation of aluminum alloys and of practical significance, but characterization of grain subdivision in a scale much larger than the grain size and how it affects texture evolution is still lacking. In this work, we performed channel die compression on an annealed AA1100 aluminum sheet along the normal direction (ND) at medium strains and room temperature. Microstructure and texture were characterized by electron backscatter diffraction (EBSD). The rotation axis and the misorientation angle for the deformation texture variants were calculated. The results show that grain subdivision proceeded in all the grains but in a heterogeneous manner. The <001>||ND grains present high angle boundaries (HABs) of 15-30° without rotation axis clustering and almost no extra high angle boundaries (EHABs) of 30-60°; while the HABs and the EHABs coexisted in the <011>||ND and the <112>||ND grains. The rotation axes of the EHABs preferentially clustered at <011> and <111>. Under plain strain compression, multiple deformation texture variants created by grain subdivision interweaved with each other inside original grains, resulting in the EHABs with rotation axes clustering. In contrast, the HABs generated by grain subdivision via dislocation mechanism showed no rotation axes clustering. Grain subdivision leveraged in the texture component intensity and randomized orientations, resulted in fluctuation of the α-fiber texture.

Introduction

During straining of high stacking fault energy (SFE) face-centered cubic (fcc) metals, e.g. aluminum and its alloys, significant change in microstructure known as grain subdivision is commonly observed [1-4]. Grain subdivision mechanisms include dislocation boundaries, noted as dense dislocation walls (DDWs), microbands (MBs), geometrically necessary boundaries (GNBs), or incidental dislocation boundaries (IDBs); between these boundaries are dislocation cells inside the original grains [1-8]. The misorientation between substructural boundaries increases with strain and eventually these boundaries evolve into high angle boundaries (HABs) (>15°) that subdivide the original grains. Extensive studies have been carried out on dislocation boundary alignment on active slip planes and/or the planes with maximum stress and the dislocation configurations with respect to original grain orientation [1-6,9,10]. Although whether DDWs/MBs lie in active {111} slip plane or the planes with maximum stress remain debatable, it is clear that dislocation boundaries subdivide the original grain, and the misorientation across the dislocation boundary increases with increasing strain [5-6,11]. Hughes and Hansen [12] investigated the HAB mechanism by transmission electron microscopy (TEM) in heavily rolled nickel and aluminum alloys (rolled to 70%-98%). They pointed out that HABs developed at high strains were mainly induced by two mechanisms: the microstructure mechanism and the texture mechanism [12]. Also using TEM, Sun et al. [13] studied formation of HABs by grain subdivision in severely deformed aluminum via equal channel angular extrusion (ECAE). Delannay et al. [14] investigated grain subdivision by electron backscatter diffraction (EBSD) in a rolled commercial purity aluminum at 40% strain and they found that the misorientation distribution is different in differently oriented parent grains.

Annealed aluminum alloys usually develop strong cube texture before cold-rolling is performed in industry. As such, understanding how microstructure and texture change during cold-rolling of strong cube-textured aluminum alloy is of significance for property control. At moderate strain, grain subdivision would significantly propagate and dominate the microstructure [7]. However, there is limited result in literature about how grain subdivision proceeds in detail in a strong cube-textured polycrystalline aluminum alloy and affects texture evolution at medium strains, typical of 40-70% under cold-rolling. Chowdhury [15] have studied the microstructure and texture evolution in cube-oriented polycrystalline aluminum during cold rolling, but detail grain subdivision behavior was not reported there.

Previous TEM studies have provided valuable insights on the nature of the subboundaries, but the statistics is poor because of the tiny sampling volume. Particularly, the correlation between grain subdivision and texture evolution needs further characterizations in a scale that is much larger than the average grain size. The main purposes of this study are to investigate the grain subdivision mechanisms at medium strains in an annealed aluminum alloy under plane strain compression, and its effect on texture evolution by statistical measurements using EBSD and calculations.

Experimental

A commercial aluminum AA1100 sheet (0.15 Si, 0.53 Fe, 0.07 Cu, 99.2 Al, wt%) with a thickness of 6 mm and a H14 status was selected as the experimental material. Samples with dimensions 10(RD)×6(ND)×4.5(TD) mm were cut from the sheet (RD - rolling direction, ND - normal direction, and TD - transverse direction). The as-cut sample was heated up to 400 °C in a furnace and held on for one hour. Then the sample was immediately quenched in water to preserve the microstructure and served as the initial sample. The initial sample was conducted plane strain compression in a channel die at room temperature on an INSTRON 5869 at a strain rate of 10^{-3} s^{-1} to three intermediate

strains: 40% (ε=-0.51), 51% (ε=-0.71), and 67% (ε=-1.11), respectively. A lubricant TEFLON film was used to limit the friction during deformation. The loading direction was along the ND direction, the flow direction was alng the RD direction, and the flow in TD was constrained.

The compressed sample was cold mounted and the RD-ND section (the longitudinal plane) of the sample was subsequently polished by a series of SiC papers down to grit number 4000, then was polished using an alumina (down to 0.05 μm) suspended in ethylene glycol. Finally the sample was polished in a vibratory polisher using a colloidal silica suspension (0.02 μm) for four hours. The polished sample without etching was then conducted EBSD scan in a high resolution field emission gun scanning electron microscope (ZEISS SUPRA-40 FEG-SEM) with TSL OIM 5.3 EBSD data collection and analysis software package. For the acquisition of texture, a large area of 1200×1200 μm in the center of RD-ND section was scanned by EBSD with a step size of 2 μm; for microstructure analysis, a fine step size of 0.2 μm was used in EBSD scan.

Results

Figure 1 presents the EBSD inverse pole figure (IPF) maps of the AA1100 samples at strain of 0% (initial), 40%, 51%, and 67%. The initial microstructure exhibits rough equiaxed grain structure with a strong <001>∥ND fiber texture (Figure 1a). Due to the strong cube texture, a considerable portion of the grain boundaries (GBs) are low angle GBs (<15°) (Figure 1a). The grains evolve into pancake at 40%, and substructure and subboundary quickly develop at strain of 51% and 67% (Figures 1b-1d). Grain size distribution at different strains is presented in Figure 2. The big grains (>50μm) occupy large area fraction in the initial sample, and small grains (<20μm) and big grains coexist at strain of 40% and 51%. There are few big grains left and small grains dominate the structure at 67% (Figure 2). Grain subdivision can be clearly seen at all three stains (Figure 1), and be confirmed by grain size distribution (Figure 2).

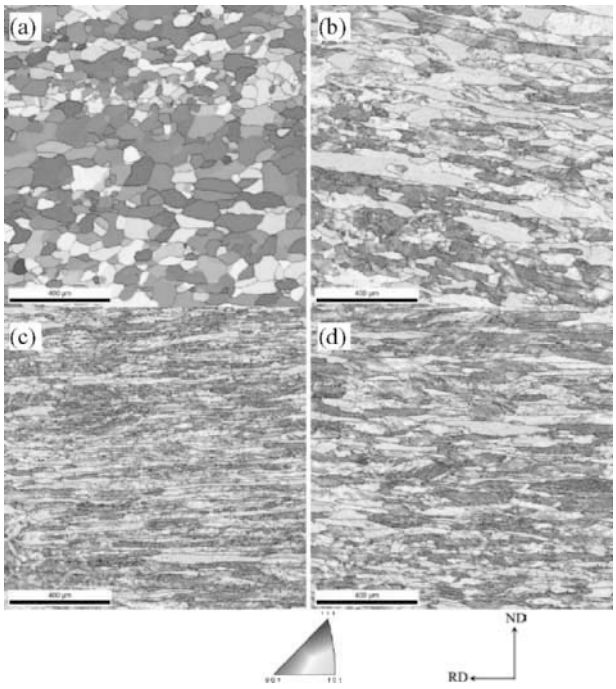

Figure 1: EBSD inverse pole figure (IPF) maps of AA1100 under plain strain compression at different strains. (a) 0%; (b) 40%; (c) 51%; (d) 67%. The black sold lines represent the boundaries with misorientation angle >15°. The typical color triangle represents the normal direction (ND). EBSD step size: 2μm.

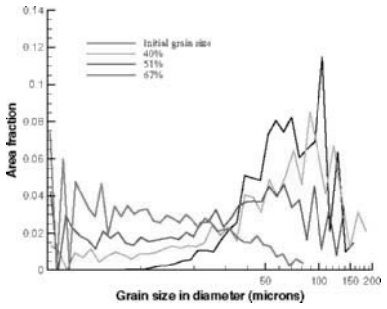

Figure 2: AA1100 gain size distribution at different strains based on EBSD scans in Figure 1. The fraction of big grain (>50 μm) decreases while the fraction of fine grain (<20 μm) increases with strain increasing from 40% to 67%. At 67%, there are few grains >50 μm left. Grain subdivision occurs from 40% to 67%.

The orientation distribution function (ODF) of AA1100 based on EBSD scan (Figure 1) was calculated using the texture software MTEX [16] with a Kernel half-width of 5°. Since φ_2=45° ODF section is the important section for fcc alloys where main texture components can be seen, the φ_2=45° ODF sections of the AA1100 at different strains are presented in Figure 3. The initial annealed AA1100 indeed has a strong cube texture. Additionally, very weak copper and brass components can be seen (Figures 3a,3e). At 40%, brass, Goss and copper strengthen, while cube texture quickly weakens (Figure 3b). At 51%, brass and Goss almost disappear, meanwhile copper slightly strengthen and cube texture continues to decrease (Figure 3c). At 67%, copper seems steady, Goss and brass increase again and the <011>∥ND texture (α-fiber) spreads widely, cube texture keeps decreasing slowly (Figure 3d).

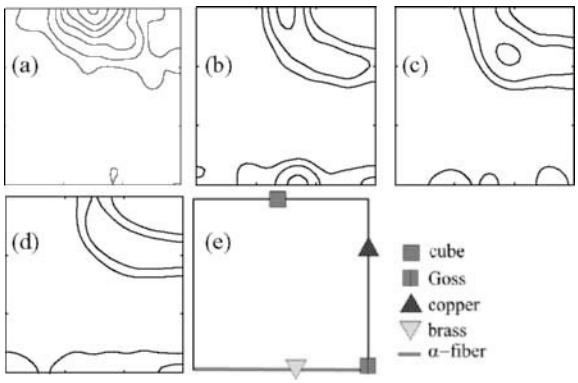

Figure 3: φ_2=45° ODF sections of the AA1100 at different stains. (a) 0%; (b) 40%; (c) 51%; (d) 67%; and (e) main texture components positions in φ_2=45° ODF section. Levels:1,2,4,6,8,10,12.

To investigate the behavior of cube-oriented grains, we highlight the <001>∥ND grains (denoted as <001> grains hereafter) with a tolerance of 15° as presented in Figure 4. The corresponding correlated misorienation (one orientation with its neighbor) angles and rotation axis-angle pairs are also presented in Figure 4d. Since grain subdivision is mainly caused by HAB, here we only show the misorientation >15° distribution, and an example of the

rotation axis distribution at rotation angle of 20±2.5°, 50±2.5°, and 60±2.5° at strain of 67% is shown in Figure 4d.

In the <001> grains, the high angle misorientation (>15°) number fraction increases with strain (Figure 4d). Meanwhile the <001> grains decompose and the size of remain <001> grains decreases with strain (Figures 4a-4c). The HABs in <001> grains mainly locate in the misorientation range of 15-30°, almost no extra high angle boundaries (EHABs) >30° exist in <001> grains. The rotation axis distribution at 20 ° shows that the rotation axes have no preferred clustering (Figure 4d).

Since the brass {011}<211> and the copper {112}<111> are the two important orientations in deformed aluminum [17], investigation behavior of the <011> ∥ ND grains and <112> ∥ ND grains (designated as <011> and <112> grains, respectively, hereafter) is of significance for the relationship between grain subdivision and texture. The <011> and <112> grains are highlighted similarly, and the corresponding high angle misorientation and rotation axis-angle distributions are plotted in Figures 5 and 6, respectively.

Similar to the <001> grains, the number fraction of the HAB of 15-30° increases in <011> and <112> grains with strain increasing (Figures 5d,6d). The rotation axes in rotation angle of 15-30° show no preferred axis (Figures 5d, 6d). However, in contrast to the <001> grains, the EHAB of 30-60° appears and its number fraction increases with strain and the rotation axes preferentially cluster at <111> and <011> (Figures 5d, 6d).

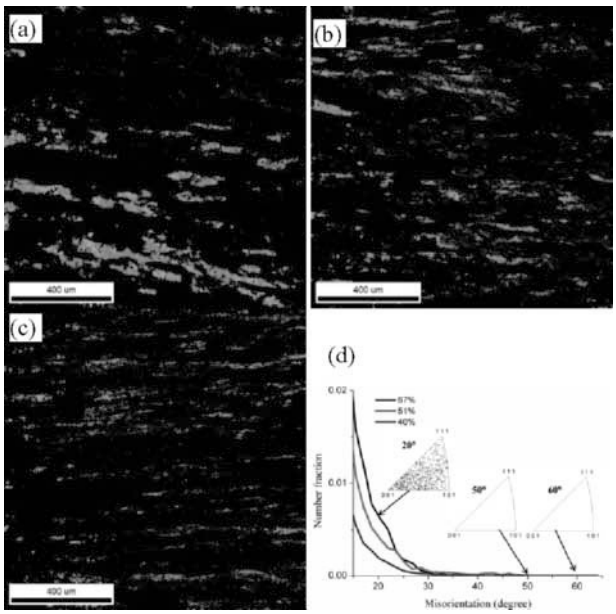

Figure 4: The highlighted <001>∥ND with a tolerance of 15° grains at three strains of (a) 40%; (b) 51%; (c) 67%, and (d) the corresponding correlated large misorientation angle (>15°) distribution and the rotation axis distribution at 20±2.5°, 50±2.5°, and 60±2.5° at 67%. Other oriented grains in Figures 4a,4b, and 4c were excluded (black areas). EBSD step size: 2μm.

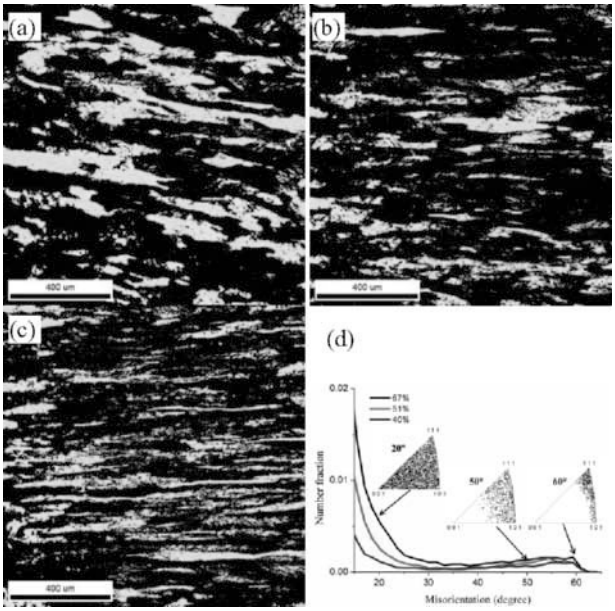

Figure 5: The highlighted <011>∥ND with a tolerance of 15° grains at three strains of (a) 40%; (b) 51%; (c) 67%, and (d) the corresponding correlated large misorientation angle (>15°) distribution and the rotation axis distribution at 20±2.5°, 50±2.5°, and 60±2.5° at 67%. Other oriented grains in Figures 5a, 5b and 5c were excluded (black areas). EBSD step size: 2μm.

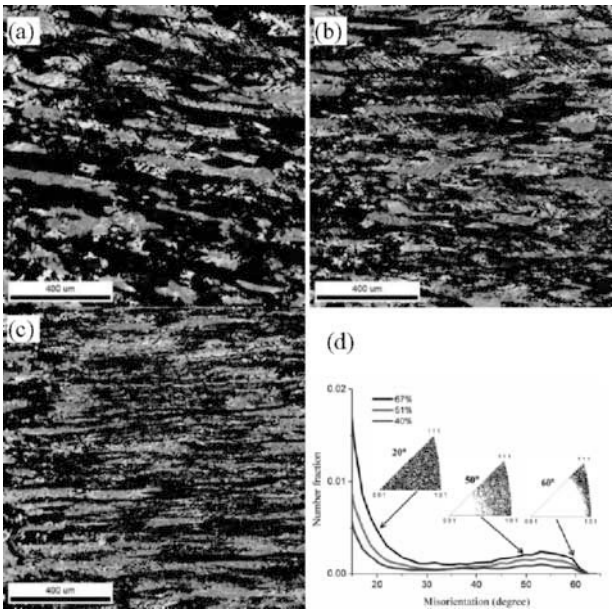

Figure 6: The highlighted <112>∥ND with a tolerance of 15° grains at three strains of (a) 40%; (b) 51%; (c) 67%, and (d) the corresponding correlated large misorientation angle (>15°) distribution and the rotation axis distribution at 20±2.5°, 50±2.5°, and 60±2.5° at 67%. Other oriented grains in Figures 6a, 6b and 6c were excluded (black areas). EBSD step size: 2μm.

Discussion

Grain subdivision mechanisms and heterogeneity

Based on EBSD results (Figures 4-6), the HABs of 15-30° increase with strain which is consistent with the scaling hypothesis (average misorientation angle increases with increasing strain) for IDB (i.e. cell boundary) misorienation

distribution in deformed fcc alloys based on extensive TEM results [18,19]. The <001> grains only exhibit the cell structure, but other oriented grains hold both cell and extended planar boundaries according to the TEM observations in the compressed aluminum [10]. The misorientation angle induced by the assumed dislocation mechanism may reach up to 15-30° [12]. Activation of multiple slip systems and grain interaction may partially stabilize the <001> grains during channel die compression [18-22]. In addition only cell structure exists in <001> grains [10]. This explains why the <001> grains only show the HABs of 15-30°.

The grain subdivision is inhomogeneous in texture point of view. The <001> grains have almost no EHABs, while <011> and <112> grains hold EHABs of 30-60° (Figures 4d,5d,6d). The <011> and <112> grains locate in the orientation space from α- to β-fiber in fcc aluminum. It is accepted that orientations tend to transform from brass via S to copper in aluminum during plane strain compression. The <011> and <112> grains experience grain subdivision as well, and can only transfer to other deformation texture variants with random orientations. Thus, different deformation texture variants evolve in the original grain and impinge each other where EHAB occurs. The orientation dependence of EHAB of 30-60° distribution could be one reason why the misorientation scaling hypothesis showed a visible deviation when all kinds of dislocation boundaries are considered [12,19]. Thus, the EHAB of 30-60° preferentially existing in <011> and <112> grains with preferred rotation axes (Figures 5d,6d) is attributed to the multiple subdivided deformation texture variants via grain subdivision.

Figure 7 shows the substructure and two lines point-point misorientation profiles in AA1100 at strain 40%. Grain subdivision occurrence was confirmed by the substructure and many >15° subboundaries (Figures 7a,7b). The substructure and subboundary are heterogeneous in different oriented grains. For example, it seems that only cell structure can be seen in <001> grains, but cell boundaries and MBs coexist in <011> grain; while some other oriented grains hold less substructures (Figure 7a). Moreover, grain subdivision exhibits intragranular heterogeneous. For example, the Line B area (grain boundary area) has dense substructures, but few substructures appear in the interior of the grain (Figure 7a). Figure 7b clearly confirms that HABs and EHABs, indeed are mainly created by grain subdivision [23]. The reason of grain subdivision heterogeneity could be attributed to the combination effect of grain orientation and local grain interaction with its neighboring grains [4,24,25].

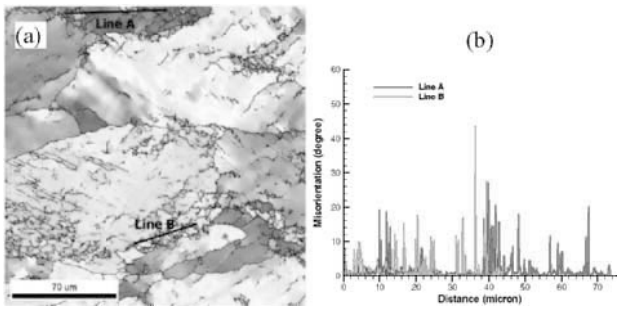

Figure 7: Grain subdivision heterogeneity in AA1100 in EBSD inverse pole figure (IPF) maps. (a) 40%, grain subdivision occurs, and propagates in both intragranular and intergranular heterogeneous styles; (b) the point-point misorientation profile of Line A and B shows >15° boundary within the <011> grain and the <001> grain.The thin solid black lines in (a) represent the boundaries with misorientation angle >5°. EBSD step size: 0.2μm.

Grain subdivision effect on texture

Due to grain subdivision, texture evolves accordingly. At strain of 40%, large amount of cube has transferred to other orientations including brass, copper and Goss (Figures 3a,3b). The quick decrease of cube texture may originate from three reasons: 1) the initial big grain size quickens up the grain subdivision [7]; 2) high density low angle GBs among cube-oriented grains favors the subdivision of cube texture (Figure 1a); and 3) the most favorable slip system may dominate plasticity at early stage (<40%) and result in quick rotation away from cube. Goss is a transition component between cube and brass, thus it is also enhanced at strain of 40% (Figure 3b). As strain increasing up to 51%, however the brass and Goss disappear, while copper slightly increases and cube slowly decreases (Figures 3b,3c). Strikingly, the brass and Goss strengthen again at 67% (Figure 3d). Hence, a fluctuation in the α-fiber texture is observed (Figure 3).

Subdivision continues in the deformation texture components. A single brass crystal was proven to be stable under channel die compression because the two slip systems have the same maximum Schmid factor, and simultaneously activate and cancel out the brass crystal rotation [26,27]. However, the active two slips lead to a strong shear strain $\varepsilon_{RD\text{-}TD}$ which renders brass unstable [14,26-28]. Thus in polycrystal case, only the two slips activation in brass are actually impossible. Under plane strain compression, if brass subdivides into brass 1 and brass 2, the signs of the shear strain $\varepsilon_{RD\text{-}TD}$ of brass 1 and brass 2 are opposite and the total $\tau_{RD\text{-}TD}$ is minimized. Similar to brass, copper would subdivide into copper 1 and copper 2 to eliminate the strong shear strain $\varepsilon_{RD\text{-}ND}$ due to the four slips activation in the copper grain [28-30]. Since both brass 1 and brass 2 belong to brass texture, brass still has a strong intensity at 40% (Figure 3b). However, with strain increasing, brass1 and brass 2 continue to subdivide. During the breakup of the brass-oriented grain into new non-brass grain (e.g. S texture variants) [27], brass texture quickly weakens due to the grain subdivision (Figure 3c). Copper still slowly increases due to the transformation from S to copper; meanwhile grain subdivision proceeds in copper, thus slows down the rate of copper increasing. The origin of the re-enhancement of the α-fiber with a wide spread at 67% may result from further deformation that causes the subdivided grains to re-aggregate along the α-fiber. The α-fiber texture fluctuation at strains 40%, 51% and 67% may presumably result from the cycle of grain subdivision with strain: grain subdivision — texture weakness — dislocation accumulation — texture enhancement — grain subdivision. In fact, the volume fraction of brass and Goss measured by X-ray diffraction in a rolled aluminum alloy was observed markedly fluctuant in the reduction from 20% to 75% [5]. Only grain subdivision can rationalize this α-fiber texture fluctuation. This texture fluctuation would subside when the grain size reduces down to the critical grain size at high strains where grain subdivision may no longer proceed [7]. The slow decrease trend of cube from 40% to 67% (Figures 3b-3d) confirms that cube indeed has partial stability during compression [20-22, 31].

Grain subdivision effect on extra high angle boundary (EHAB)

Because grain subdivision continues during deformation, the deformation texture components evolve to different variants. These texture variants in Bunge Euler angle $\{\varphi_1, \Phi, \varphi_2\}$ are: brass 1 {35,45,0}, brass 2 {325,45,0}, copper 1 {90,35,45}, copper 2

{270,35,135}, S 1 {60,32,65}, S 2 {300,148,245}, S 3 {120,148,245}, S 4 {240,32,65}. In a fine EBSD scanning map at 67% (Figure 8a), these different deformation texture variants and the cube in fcc aluminum are colored by their specific orientations (Euler angles) with a tolerance of 20°. Substructures with other orientations (no deformation texture variants and the cube) shown in white are considered as random component (Figure 8a). The orientation map at 67% (Figure 8a) substantially confirms that different deformation texture variants are created by grain subdivision. These subdivided deformation texture variants interweave each other inside a grain (Figure 8a). Moreover, the random texture colored in white in Figure 8a appears to be significant as a result of grain subdivision. Orientation randomization by grain subdivision leads to the lower deformation texture intensity.

Theoretically, there are 36 different neighboring pairs among the deformation texture variants: Goss, brass 1, brass 2, copper 1, copper 2, S 1, S 2, S 3, and S 4. The misorientation and the corresponding rotation axis of the 36 neighboring pairs are calculated by MTEX [16] and plotted in Figure 8b. Note that the misorientation angle (i.e. the disorientation angle) is the smallest misorientation angle among the 24 variants in fcc aluminum. A large number fraction of misorientation angle in 30-60° can be seen, in addition, the corresponding rotation axes preferentially clusters at <111> and <011> (Figure 8b). The calculated misorientation and rotation axis distribution are consistent with the measured EHAB misorientation and the corresponding rotation axis distribution in <011> and <112> grains (Figures 5d,6d,8b). The number fraction of these texture variants increases with strain due to further grain subdivision. This is the reason why the fraction of EHAB of 30-60° misorientation increases with strain in <011> and <112> grains (Figures 5d,6d). The calculated and experimental results confirm that the EHABs indeed result from grain subdivision in the deformation texture components. According to calculation and experimental observations, the HABs of 15-30° mainly result from grain subdivision by dislocation mechanism [12], while the EHABs of 30-60° are mainly induced by grain subdivision proceeding in the deformation textures. It is conceivable that if the deformation mode changes, e.g. simple tension or torsion, then deformation textures will change accordingly. Thus, grain subdivision may proceed differently. Moreover, the effect of grain subdivision may be negligible after high strain deformation because there is little subdivision at high strains [7]. Therefore, typical deformation textures may normally develop and enhance after high strain deformation.

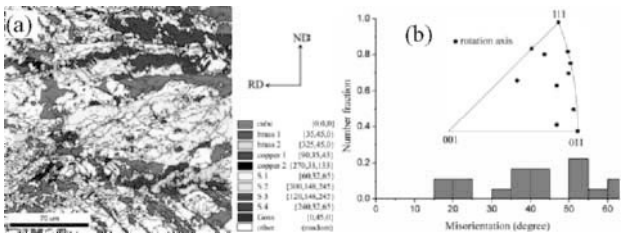

Figure 8: (a) Subdivided texture variants interweave each other during grain subdivision at 67%. The color rectangles are the orientation legends that represent the specific texture components within 20° of ideal orientations. The solid black lines are the boundaries with a misorientation angle >5°. (b) The distribution of the misorientation angle and rotation axis of the 36 pairs of the ideal deformed texture variants in fcc aluminum. The texture variants include: Goss {0,45,0}, brass 1 {35,45,0}, brass 2 {325,45,0}, copper 1 {90,35,45}, copper 2 {270,35,135}, S 1 {60,32,65}, S 2 {300,148,245}, S 3 {120,148,245}, and S 4 {240,32,65}. The results show that most of misorientation angle locates in 30-60° and the rotation axis preferentially clusters at <111> and <011>.

Conclusions

An annealed cube-textured commercial AA1100 aluminum alloy was conducted channel die compression to strain of 40%, 51% and 67%, respectively. The microstructure and texture of the AA1100 samples were characterized by EBSD. The misorientation angle and the rotation axis among deformation texture variants were also calculated. Some conclusions were drawn based on experimental and calculation as follows.

1. Grain subdivision occurred in the annealed AA1100 aluminum alloy in the strain range of 40%-67%. Grain refinement was carried out by grain subdivision. Both stable and unstable oriented grains experienced grain subdivision during deformation. Grain subdivision proceeded in a heterogeneous manner due to grain orientation and grain interaction. The HABs of 15-30° and the EHABs of 30-60° at medium strains were mainly created by grain subdivision.

2. The HABs of 15-30° did not have rotation axes clustering in <001>, <011> and <112> grains and the number fraction of high angle boundary of 15-30° increased with strain. It was mainly caused by grain subdivision through dislocation mechanism in <001>,<011> and <112> grains.

3. The EHABs of 30-60° in <011> and <112> grains resulted from deformation texture variants that interweaved each other due to grain subdivision. Few EHABs were observed in the <001> grains due to the partial stability of cube and only cell structures exist in the cube.
4. Grain subdivision smoothed deformation texture intensity, randomized orientations, and resulted in fluctuation in the α-fiber texture in AA1100 aluminum alloy at medium strains.

Acknowledgements

The authors are grateful to the financial support from the Department of Energy, Contract No. DE-FC-26-06NT42755, and the Center for Advanced Vehicular Systems (CAVS) at Mississippi State University. The authors are also grateful to Robert Malley and Stephen Horstemeyer for their assistance with the experimental works at CAVS.

References

1. Q. Liu and N. Hansen, "Geometrically necessary boundaries and incidental dislocation boundaries formed during cold deformation", *Scripta Metallurgica et Materialia*, 32(1995) 1289-1295.
2. Q. Liu, et al., "Heterogeneous microstructures and microtextures in cube oriented Al crystals after channel die compression", *Metallurgical and Materials Transactions A,* 29(1998) 2333-2344.
3. G. Winther, X. Huang and N. Hansen, "Crystallographic and macroscopic orientation of planar dislocation boundaries-Correlation with grain orientation", *Acta Materialia*, 48(2000) 2187-2198.
4. N. Hansen, X. Huang and G. Winther, "Effect of grain

boundaries and grain orientation on structure and properties", *Metall Mater Trans A*, 42(2011) 613-625.
5. P.J. Hurley and F.J. Humphreys, "The application of EBSD to the study of substructural development in a cold rolled single-phase aluminum alloy", *Acta Materialia,* 51(2003) 1087-1102.
6. P.J. Hurley, P.S. Bate and F.J. Humphreys, "An objective study of substructural boundary alignment in aluminum", *Acta Materialia,* 51(2003) 4737-4750.
7. F.J. Humphreys et al., "Developing stable fine-grain microstructures by large strain deformation", *Philosophical. Transactions of the Royal Society A*, 357(1999) 1663-1681.
8. M.F. Horstemeyer and D.L. McDowell, "Modeling effects of dislocation substructure in polycrystal elastoviscoplasticity", *Mechanics of Materials*, 27(1998) 145-163.
9. F.X. Lin, A. Godfrey and G. Winther, "Grain orientation dependence of extended planar dislocation boundaries in rolled aluminum", *Scripta Materialia*, 61(2009) 237-240.
10. G.M. Le et al., "Orientation dependence of the deformation microstructure in compressed aluminum", *Scripta Materialia*, 66(2012) 359-362.
11. G. Winther et al., "Critical comparison of dislocation boundary alignment studied by TEM and EBSD: technical issues and theoretical consequences", *Acta Materialia*, 52(2004) 4437-4446.
12. D.A. Hughes and N. Hansen, "High angle boundaries formed by grain subdivision mechanisms", *Acta Materialia*, 45(1997) 3871-3886.
13. P.L. Sun, P.W. Kao and C.P. Chang, "High angle boundaries formation by grain subdivision in equal channel angular extrusion", *Scripta Materialia*, 51(2004) 565-570.
14. L. Delannay et al., "Quantitative analysis of grain subdivision in cold rolled aluminum", *Acta Materialia*, 49(2001) 2441-2451.
15. S.G. Chowdhury, "Development of texture during cold rolling in AA5182 alloy", *Scripta Materialia*, 52(2005) 99-105.
16. R. Hielscher and H. Schaeben, "A novel pole figure inversion method: Specification of the MTEX algorithm", *Journal of Applied Crystallography,* 41(2008) 1024-1037.
17. W. Mao, "Modeling of rolling texture in aluminum", *Materials Science and Engineering A*, 257(1998) 171-177.
18. D.A. Hughes et al., "Scaling of misorientation angle distributions", *Physical Review Letters*, 81(1998) 4664-4667.
19. D.A. IIughes et al., "Scaling of microstructural parameters: misorientations of deformation induced boundaries", *Acta Materialia*, 45(1997) 105-112.
20. I. Samajdar and R. Doherty, "Cube recrystallization texture in warm deformed aluminum: understanding and prediction", *Acta Materialia*, 46(1998) 3145-3158.
21. F. Basson and J.H. Driver, "Deformation banding mechanisms during plane strain compression of cube-oriented fcc crystals", *Acta Materialia*, 48(2000) 2101-.
22. P. Mukhopadhyay and S. Badirujjaman, "Relative stability of cube orientation in single crystal aluminum during deformation", *Trans Indian Inst Met*, 65(2012) 343-353.
23. D.A. Hughes and N. Hansen, "High angle boundaries and orientation distributions at large strains", *Scripta Metallurgica et Materiala,* 33(1995) 315-321.
24. D. Raabe, Z. Zhao and W. Mao, "On the dependence of in-grain subdivision and deformation texture of aluminum on grain interaction", *Acta Materialia*, 50(2002) 4379-4394.
25. W.C. Liu and P.P. Zhai, "Characterization of microstructures near grain boundary in hot deformed AA3104 aluminum alloy", *Materials Characterization*, 62(2011) 81-89.
26. A. Albou, J.H. Driver and C. Maurice, "Microband evolution during large plastic strains of stable {110}<112> Al and Al-Mn crystals", *Acta Materialia*, 58(2010) 3022-3034.
27. A. Ray and B.J. Diak, "Grain interaction effect on the stability of the {110}<112> "brass" orientation in an aluminum multi-crystal", *Scripta Materialia*, 62(2010) 606-609.
28. J.H. Driver, J.H. Jensen and N. Hansen, "Large strain deformation structures in aluminum crystals with rolling texture orientations", *Acta Metallurgica et Materialia* , 42(1994) 3105-3114.
29. A. Godfrey, J.H. Jensen and N. Hansen, "Slip pattern, microstructure an local crystallography in an aluminum single crystal of Copper orientation {112}<111>", Acta Materialia, 46(1998) 835-848.
30. P. Wagner, O. Engler and K. Lücke, "Formation of Cu-type shear bands and their influence on deformation and texture of rolled fcc {112}<111> single crystals", *Acta Metallurgica et Materialia* , 43(1995) 3799-3812.
31. Q. Ma et al., "Rapid texture measurement of cold-rolled aluminum sheet by X-ray diffraction", *Scripta Materialia*, 54(2006) 1901-1906.